Mechanics of Slip and Fracture Along Small Faults and Simple Strike-Slip Fault Zones in Granitic Rock

STEPHEN J. MARTEL

Earth Sciences Division, Lawrence Berkeley Laboratory, Berkeley, California

DAVID D. POLLARD

Departments of Applied Earth Sciences and Geology, Stanford University, Stanford, California

We exploit quasi-static fracture mechanics models for slip along pre-existing faults to account for the fracture structure observed along small exhumed faults and small segmented fault zones in the Mount Abbot quadrangle of California and to estimate stress drop and shear fracture energy from geological field measurements. Along small strike-slip faults, cracks that splay from the faults are common only near fault ends. In contrast, many cracks splay from the boundary faults at the edges of a simple fault zone. Except near segment ends, the cracks preferentially splay into a zone. We infer that shear displacement discontinuities (slip patches) along a small fault propagated to near the fault ends and caused fracturing there. Based on elastic stress analyses, we suggest that slip on one boundary fault triggered slip on the adjacent boundary fault, and that the subsequent interaction of the slip patches preferentially led to the generation of fractures that splayed into the zones away from segment ends and out of the zones near segment ends. We estimate the average stress drops for slip events along the fault zones as ~1 MPa and the shear fracture energy release rate during slip as 5×10^2 - 2×10^4 J/m^2. This estimate is similar to those obtained from shear fracture of laboratory samples, but orders of magnitude less than those for large fault zones. These results suggest that the shear fracture energy release rate increases as the structural complexity of fault zones increases.

INTRODUCTION

Structural geologists have only recently applied principles of fracture mechanics and elasticity theory to the development of natural fracture systems. Most studies have focused on dilatant structures such as dikes [*Delaney and Pollard*, 1981; *Pollard et al.*, 1983; *Rubin and Pollard*, 1987] and joints [*Ryan and Sammis*, 1978; *Kulander et al.*, 1979; *Segall*, 1984; *Degraff and Aydin*, 1986]. This study applies principles of fracture mechanics and elasticity theory to help understand how slip occurs and fractures develop along small faults and simple fault zones in granitic rock. Theoretical and experimental studies of fault mechanics have tended to focus on either large, well-developed fault zones or fractures in relatively small samples. The factors controlling the propagation of shear displacement discontinuities have been considered primarily in the context of earthquake processes along major faults [e.g., *Ida*, 1973; *Andrews*, 1976; *Freund*, 1979; *Rudnicki*, 1980; *Li*, 1987]. The theoretical elastic effects of faulting at this scale have been discussed in the context of aftershocks [*Stein and Lisowski*, 1983], geodetic deformation [*Thatcher*, 1979; *Harris and Segall*, 1987], and the generation of secondary faults and extension fractures [*Rodgers*, 1980; *Segall and Pollard*, 1980; *Sibson*, 1985]. Laboratory studies on the energy for dilatant fracture [*Brace and*

Walsh, 1962; *Friedman et al.*, 1972; *Ingraffea*, 1981; *Atkinson*, 1984; *Peck et al.*, 1985a, b; *Meredith and Atkinson*; 1985; *Atkinson and Meredith*, 1987] and for shear fracture [*Wong*, 1982, 1986; *Li*, 1987] have dealt principally with initially intact samples with maximum dimensions of several centimeters. The largest laboratory samples in which shear fracture has been studied are 1.5 m on a side [*Okubo and Dieterich*, 1981, 1984].

We have used findings from these large-scale and small-scale studies to help understand slip and fracturing processes along natural faults and fault zones at the outcrop scale. We first develop models for how slip might occur along small faults and simple fault zones. From these models we estimate stress drop and shear fracture energy from geological field measurements. The small strike-slip faults and simple strike-slip fault zones we consider here are found in granitic plutons of the Mount Abbot quadrangle in California (Figure 1). These faults and fault zones may have been active at depths of several kilometers [*Martel et al.*, 1988], similar to focal depths along presently active fault zones in granitic basement, such as the San Andreas.

STRUCTURAL SETTING

Previous work [*Segall and Pollard*, 1983b; *Martel* et al., 1988] has shown that small faults and simple fault zones in the Mount Abbot quadrangle developed in a multi-stage sequence from pre-existing joints (Figure 2a). The joints
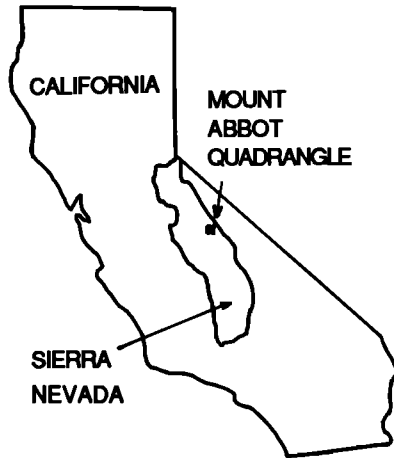
Fig. 1. Index map showing the location of the Mount Abbot quadrangle.

formed in domains with horizontal dimensions of several tens to a few hundreds of meters. Joint strikes vary by only a few degrees within a domain [Segall and Pollard, 1983a], but differ in strike by as much as 20° in adjacent domains. With the exception of some small steps and bends, the traces of joints are nearly linear on both horizontal and vertical surfaces, indicating that the joints are approximately planar. The joints are as much as a centimeter wide and several tens of meters long. Joint spacing ranges from a few decimeters to a few tens of meters. Those joints not involved in later faulting contain undeformed hydrothermal minerals, predominantly epidote and chlorite.

Small left-lateral faults developed next as the opposing walls of some joints slipped relative to one another (Figure 2b). The small faults left-laterally offset steeply-dipping markers as much as 2 m. Subhorizontal slicken-lines on the small faults indicate that at least the most recent displacement across the faults has been nearly pure strike-slip. In response to slip, the material in the small faults acquired mylonitic fabrics [Segall and Pollard, 1983b, Segall and Simpson, 1986]. Dilatant fractures, which we refer to as splay cracks, grew away from the ends of many faults. Splay cracks usually extend no more than a few meters from fault ends and generally strike 15°-35° counterclockwise from the fault planes. Like the joints, the splay cracks contain undeformed epidote and chlorite, but many also contain quartz. Splay cracks linked some adjacent left-stepping echelon faults end-to-end, thus transferring slip by brittle fracture. Apparently, slip also was transferred between some right-stepping echelon faults by ductile deformation of the intervening granodiorite [Segall and Pollard, 1983b]. Some echelon faults linked together to form structures more than 100 m long that accommodated several meters of left-lateral separation.

Simple fault zones developed as abundant oblique fractures linked two adjacent small faults side-to-side (Figure

2c). These zones left-laterally offset steeply-dipping markers as much as 10 m. They typically are half a meter to 3 m wide and hundreds of meters long. The shear displacement across a simple fault zone is concentrated on the pre-existing faults that bound the zone. The material in these boundary faults is characterized by cataclastic microtextures, in contrast to the mylonitic material in small faults. Martel et al. [1988] account for the cataclastic texture by suggesting that the boundary faults experienced a higher shear strain rate than the small faults, as opposed to a greater shear strain or slip under lower temperature/pressure conditions.

Simple fault zones more than 100 m long consist of noncoplanar segments a few tens of meters long that join at steps or bends [Martel et al., 1988, Figure 9b]. Steps link parallel echelon segments and bends link segments with different strikes (Figure 2c). The segmentation reflects the initial distribution of the joints. The nearly equal strike-slip separations of dikes offset at contiguous fault zone segments indicate that displacement was transferred effectively from one segment to the next. The rock outside fault zones usually is highly fractured only at segment ends; away from segment ends, external fractures are relatively scarce. In contrast, fractures are abundant inside the fault zones.

The most prominent internal fractures in the simple fault zones are either straight or very gently curved, and they strike at acute counterclockwise angles from the boundary faults [Martel et al., 1988, Figure 8b]. They typically are spaced 1-20 cm apart. Like the splay cracks near the ends of small faults, the internal fractures contain epidote, chlorite, and quartz. The fractures commonly intersect one or both of the boundary faults, but nowhere have we observed the fractures to cross or offset the boundary faults. These observations indicate that the most prominent internal fractures nucleated and, in some cases, terminated along the boundaries. Thus, like the splay cracks, the most prominent internal fractures appear to have grown as dilatant fractures, although some subsequently accommodated shear displacements [Martel et al., 1988, Figures 7 and 12].

We can rule out a few possible causes for the extensive fracturing within simple fault zones. Small irregularities in fault geometry did not lead to extensive fracturing along isolated small faults and presumably were of little significance in developing fracturing along boundary faults. The boundary faults originated as joints, and because deformation fields are symmetric about opening mode fractures [Pollard and Segall, 1987], it seems most unlikely that the rock on one side of a joint (the eventual inside of a fault zone) would become preferentially weaker than the rock on the other side (the eventual outside). Envisioning the rock within the fault zones as being "ground up" between two large rock masses slipping past one another also may be misleading. Given that the rock strengths originally were the same, the rock inside and outside the fault zones should have been damaged about equally by such slipping. The mechanism(s) that caused
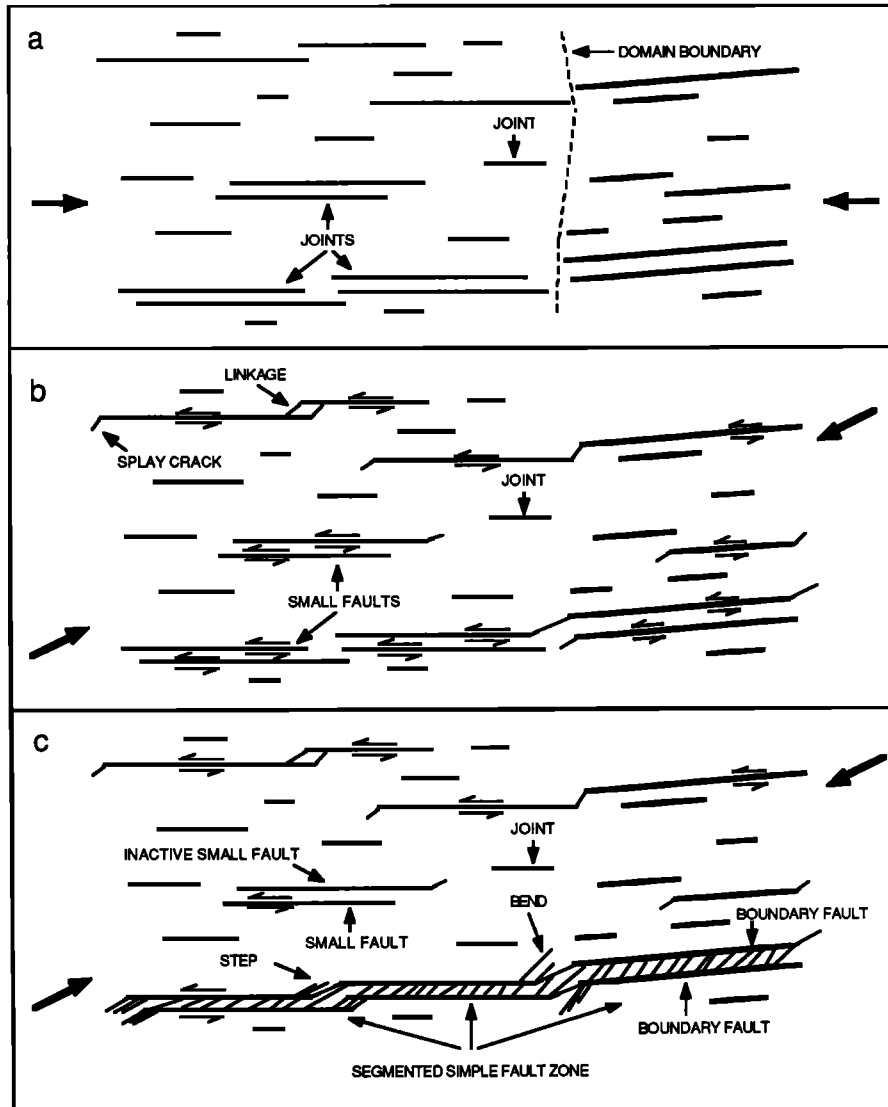
Fig. 2. The first three stages of faulting in the Mount Abbot quadrangle. Heavy arrows indicate inferred direction of maximum horizontal compressive stress. (a) Opening of joints. (b) Development of small left-lateral faults. Splay cracks form near the ends of some faults and some faults become linked. (c) Development of simple fault zones as extensive fracturing develops between some closely spaced faults.

fracturing in the fault zones away from segment ends allowed the rock outside the zones to remain largely unfractured.

Some fracturing of the rock within the fault zones probably occurred as the rock was displaced past the major geometric irregularities at the end of fault zone segments. However, this mechanism can account only for fractures near the segment ends, for the displacement across most simple fault zones is much less than segment lengths. For example, if a fault zone with segments 40 m long accommodated 5 m of lateral displacement, then rock fractured at a segment end could be conveyed no more than 5 m from that segment end. However, along the simple fault zones we have studied, the extent of fractured rock along the fault zone segments generally far exceeds the accommodated lateral displacement. This suggests that most of

the fractures along simple fault zones were not formed at segment ends and then subsequently displaced. Another mechanism is needed to account for the fractures that occur well away from segment ends. The mechanical interaction of two adjacent faults apparently played a key role in the fracturing. Extensive fracturing has not been observed between two joints or between a joint and a fault, but only between two faults. This indicates that slip on two side-by-side faults was necessary to produce extensive internal fracturing.

SLIP AND FRACTURING ALONG SMALL FAULTS

The small faults responded to imposed shear stress by considerable ductile deformation of the material inside the faults and by the accumulation of shear displacement between adjacent blocks of granodiorite. The key features
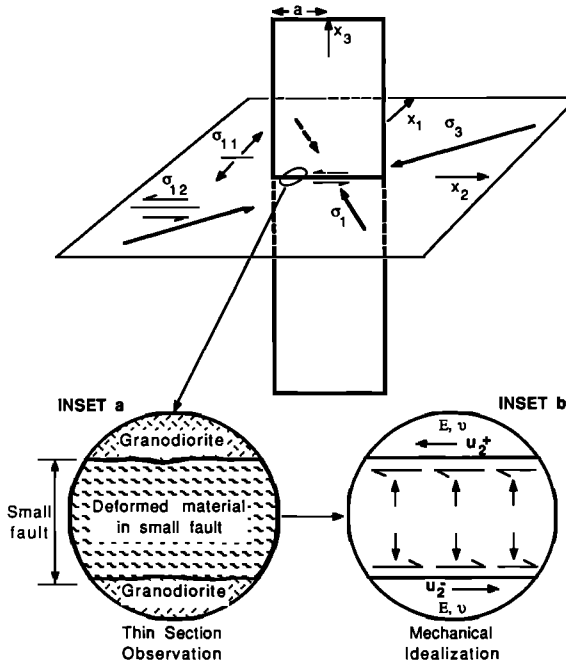
Fig. 3. Idealization of fault geometry showing the reference frame for stresses. Inset a depicts microscopic characteristics of a fault and the adjacent granodiorite. Inset b shows the effect of the fault material represented by boundary tractions (shown by arrows) and the granodiorite represented as an elastic material with Young's modulus E and Poisson's ratio v. Displacements u_2^+ and u_2^- are parallel to the fault.

of deformation outside the faults we will address are (1) the general absence of splay cracks along the central portions of these faults, (2) the presence of dilatant splay cracks near the ends of small faults, and (3) the tendency for splay cracks to form in response to slip rather than the small faults propagating on strike into the unjointed granodiorite as shear fractures.

Mechanical Idealization of Problem

We idealize the walls of a small fault as a pair of closely spaced planar surfaces with vertical dimensions much greater than their horizontal lengths, 2a (Figure 3). We postulate no variation in geometry, rock properties, or boundary conditions in the vertical dimension. Coordinates in the horizontal plane are x_2, x_1, with x_1 perpendicular to the fault plane. The stress components σ_{12} and σ_{11} act on the fault planes. The granodiorite outside a small fault is idealized as a linear elastic, homogeneous, isotropic material. We represent the deformed material inside a fault (inset a, Figure 3) by boundary tractions on the fault walls which can vary in time and in space (inset b, Figure 3). We limit the relative displacement across a fault to pure left-lateral strike-slip. Under these conditions the problem is one of two-dimensional plane strain, and the displacement and stress fields are functions only of the horizontal coordinates. We acknowledge that small faults are three-dimensional structures, but the lack of constraints on structural variation with depth and the attrac-

tive simplification of a two-dimensional model have motivated this approach.

Detailed examination of the small faults shows that their thicknesses and edge structures are not perfectly uniform along strike. The shear and normal stress components acting on the faults are also unlikely to be completely uniform along strike. Because of these heterogeneities, it seems likely that slip would nucleate more readily at a certain point or points along a fault rather than occurring simultaneously along the entire fault. Additionally, because the fault surfaces did not wear evenly and the stresses acting on the faults probably varied with time, we expect that slip would nucleate at different points along the faults through the course of time.

We hypothesize that the relative shear displacement across a small fault accumulates during a shearing or slip event. The terms u_2^+ and u_2^- refer to displacements of opposite walls of a fault (inset b, Figure 3). We consider the shear displacement field to be discontinuous across the section of a fault activated during a slip event in the sense that u_2^+ is directed oppositely from u_2^-, but acknowledge that "slip" actually may be continuous shear strain of great magnitude of the material within the fault.

For brevity, we will refer to a shear displacement discontinuity as a slip patch. We will assume that a slip patch nucleates over a small distance (Figure 4a) and then propagates along a fault in a quasi-static fashion with an accompanying increase in relative slip (Figure 4b). In fracture mechanics terms, a slip patch is analogous to a
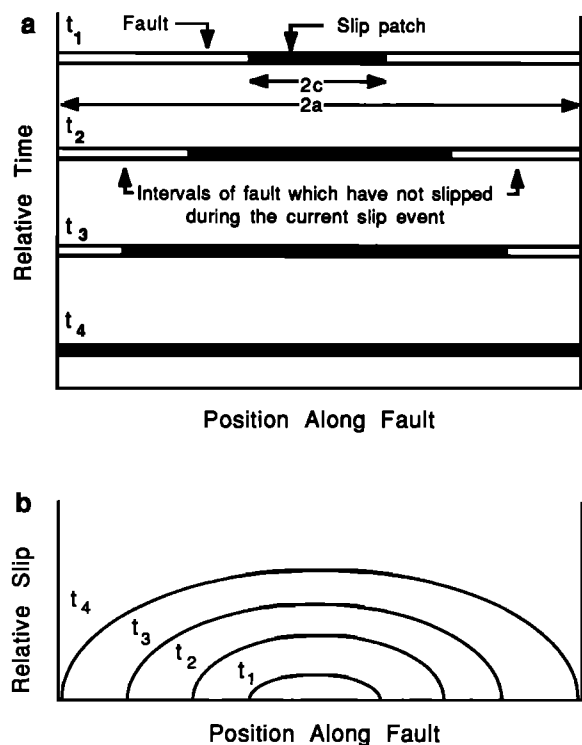

Fig. 4. (a) Representation of the nucleation (time t_1) and propagation of a slip patch (times t_2 - t_4). (b) Associated accumulation of relative slip from times t_1 through t_4.
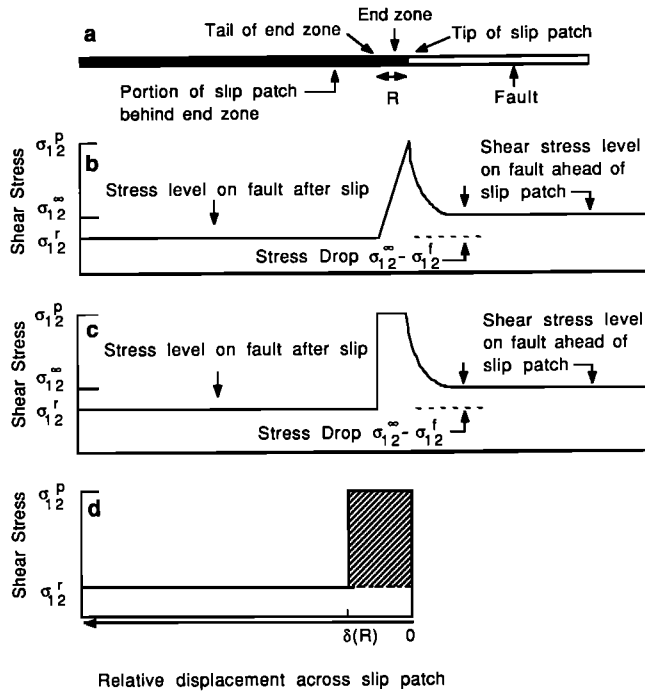
Fig. 5. Characteristics of a slip patch. (a) Elements of a slip patch. (b) Shear stress along a slip patch and along a fault ahead of a slip patch as inferred from the experiments of Okubo and Dieterich [1984]. (c) Idealization of shear stress levels along a slip patch and ahead of it. (d) Shear stress drop along a slip patch as a function of displacement across the slip patch. The shaded area is defined as the energy release per incremental unit area of crack advance. The relative shear displacement across the tip of the end zone is zero and the relative shear displacement across the tail of the end zone is δ(R).

mode II shear crack. We emphasize that it is the slip patch that propagates, and not the fault; a fault simply acts as a guide for a slip patch. The length of a slip patch 2c at a given instant in time will be less than or equal to the fault length 2a.

Details of slip patch propagation have been captured especially well in the experiments of Okubo and Dieterich [1981, 1984], and we base our model in part on their observations. In their experiments a fault was simulated by a 2-m-long lapped, sawcut surface between slabs of Sierra white granite. A biaxial frame applied a shear stress across the cut. Slip patches apparently nucleated along the cut over small distances (<40 cm). As a slip patch tip (Figure 5a) came abreast of an observation point adjacent to the cut, the shear stress there rose sharply from the ambient level σ_{12}^{∞} to a peak level σ_{12}^{p} (Figure 5b). Once the tip of a slip patch had propagated past the observation point, the shear stress dropped below σ_{12}^{∞} to a residual value σ_{12}^{r} and remained at a roughly constant level as the slip patch grew in length and as displacement increased. The quantity (σ_{12}^{∞} - σ_{12}^{r}) is referred to as the stress drop.

In keeping with the terminology of Rudnicki [1980], we call the regions at the ends of our slip patch in which $\sigma_{12} > \sigma_{12}^{r}$ the end zones (Figure 5a). The tip of the slip patch coincides with the tip of an end zone, and the tail of the

end zone is where σ_{12} has dropped to σ_{12}^{r}. Estimates of the end zone length R range from the order of several millimeters [Okubo and Dieterich, 1984] to more than 100 m [Rudnicki, 1980]. Theoretical elastic analyses [Ida, 1972; Palmer and Rice, 1973; Andrews, 1976; Rudnicki, 1980; Li, 1987] indicate that end zone length and stress level must be balanced with respect to the stress level along the rest of a slip patch in order for the stresses in front of a slip patch to remain bounded. For the case where the end zone stress level is idealized as being constant (Figure 5c), the end zone length is

$$R = (c\pi^2/8)[(\sigma_{12}^{\infty} - \sigma_{12}^{r})^2/(\sigma_{12}^{p} - \sigma_{12}^{r})^2] \qquad (1)$$

For end zone stresses that decrease linearly from σ_{12}^{p} to σ_{12}^{r}, Rudnicki [1980] indicates that the end zone length would be increased by a factor of 9/4.

Slip and Splay Fracture Formation Along the Central Portions of Small Faults

The propagation of a slip patch is driven by mechanical energy supplied by the surrounding rock. The mechanical energy that would be expended in excess of heat lost to friction (per unit area of patch growth) as a slip patch without end zones propagates in a perfectly elastic material is called the energy release rate G_{II} [Rudnicki, 1980]. If a slip patch of unit depth with small end zones advanced an incremental distance along a fault, then the shaded area beneath the stress-displacement curve in Figure 5d closely approximates G_{II} [Palmer and Rice, 1973; Rudnicki, 1980]. For the remainder of this paper we will assume that the end zone is small. With this assumption, G_{II} can also be approximated as

$$G_{II} = c\pi(\sigma_{12}^{\infty} - \sigma_{12}^{r})^2 (1-\nu)/\mu \qquad (2)$$

where ν is Poisson's ratio and μ is the shear modulus. A slip patch can propagate and slip can accumulate across it provided G_{II} equals a threshold level, the resistance to the propagation of slip G_{II}^{slip}. If G_{II} is less than G_{II}^{slip}, then the slip patch will be unable to propagate and fault slip would not accumulate. Okubo and Dieterich [1984] indicate that G_{II}^{slip} increases as the compressive stress acting across faults increases and as faults become rougher.

Another possibility is that a splay crack would form from a slip patch tip. Many experiments with brittle materials have shown that a planar crack subject to shear will tend to develop a splay crack at one or both of its ends instead of propagating in-plane [Brace and Bombolakis, 1963; Erdogan and Sih, 1963; Nemat-Nasser and Horii, 1982]. Local irregularities in fault geometry, changes in frictional strength, and changes in the compression across a small fault would cause the resistance to slip to vary along it. If a slip patch tip encounters a region where the shear strength of the fault becomes greater and the shear stress in the end zone rose, then the stress in the rock adjacent to the end zone would also rise. If the end zone shear stress rose sufficiently, then the corresponding increase in tensile stress could lead to the formation of a splay crack.

The formation of a splay crack would be favored if the fracture energy release rate required for continued slip patch propagation became locally greater than that required for splay crack formation (G^{splay}).

The scarcity of splay cracks along the central portions of small faults indicates that the propagation of slip patches usually was energetically more favorable than splay crack formation (i.e. G^{splay} usually exceeded G_{II}^{slip}). Along most small faults, local irregularities in fault geometry, increases in frictional strength, and increases in the fault-normal compression apparently were too small to cause G_{II}^{slip} to exceed G^{splay}. As a result, those slip patches that stopped propagating before reaching the ends of a fault typically did not cause splay cracks to form.

Formation of Splay Cracks at the Ends of Small Faults

The presence of splay cracks at or near the ends of small faults suggests that slip patches commonly propagated to the ends of faults. When a slip patch propagates to the end of a small fault, concentrations of tensile stress and shear stress would arise there. The plane across which the maximum shear stress would occur is the extension of the fault plane, so one might predict that a fault would propagate in-plane by shear fracture of the granodiorite. However, because splay cracks have been observed at fault ends [Segall and Pollard, 1983b], we infer that the faults did not propagate along strike as shear fractures. We conclude that the shear fracture resistance of unfaulted, unfractured granodiorite (G_{II}^{shear}) was greater than the splay fracture resistance of the granodiorite:

$$G_{II}^{shear} > G^{splay} \qquad (3)$$

This behavior also has been observed in Indiana limestone and Westerly granite in laboratory tests at room temperatures and pressures [Ingraffea, 1981].

Both experimental study [Brace and Bombolakis, 1963; Erdogan and Sih, 1963] and theoretical work [Lawn and Wilshaw, 1975; Cotterell and Rice, 1980; Pollard and Segall, 1987] indicate that splay cracks would tend to grow parallel to trajectories of maximum compressive stress. For left-lateral slip, splay cracks would form at an acute counterclockwise angle with respect to the strike of the fault (Figure 2b).

SLIP AND FRACTURING ALONG BOUNDARY FAULTS

The key aspects of fracturing along the boundary faults of a simple fault zone that we address are (1) the general absence of fractures (along the central portion of simple fault zone segments) that splay out of fault zones, (2) the abundance of fractures that splay into the zones, and (3) the abundance of fractures near the ends of fault zone segments. Because the field observations suggest that interactive slip on the boundary faults was responsible for the fracture style along the simple fault zones, we will focus on how slip (and the associated stress drop along a slip patch) on one boundary fault would tend to influence the behavior of a slip patch on the other boundary fault. To
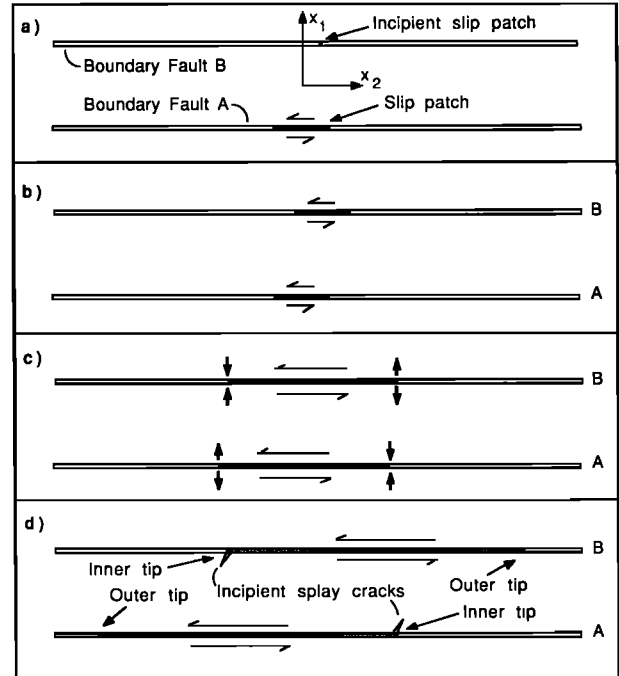

Fig. 6. Growth of left-lateral slip patches on adjacent boundary faults. (a) Slip patch nucleates on fault A. (b) Slip patch nucleates on fault B in response to slip on fault A. (c) Interaction of the slip patches as they propagate produces "stress barriers." (d) Slip patches grow into a left-lateral configuration and generate splay cracks directed into the fault zone.

isolate the stress perturbation associated with displacement across a slip patch we hold the remote shear stress constant during slip. We pay particular attention to locally induced increases in the shear stress driving slip on the faults, which increases G_{II}, and increases in the compression acting on the faults, which increase G_{II}^{slip} [Okubo and Dieterich, 1984; Wong, 1986].

We begin by considering what effect a slip patch nucleating at a point on one boundary fault (fault A, Figure 6a) would have at an adjacent point on the other boundary fault (fault B). We assume that the resistance to slip is similar at both points. This is reasonable given the similar thickness and composition of the material in boundary faults. We also assume that the normal and shear stress acting on adjacent points on the faults are similar. This is reasonable given the proximity of the points. Thus if a slip patch were on the verge of nucleating on A, a slip patch could also be on the verge of nucleating at an adjacent point on B. We now consider whether slip nucleating on A will enhance or inhibit the tendency for a slip patch to nucleate on B.

Slip across a patch on A induces changes in the normal stress perpendicular to the boundary faults (σ_{11}). The change in σ_{11} has an antisymmetric distribution (Figure 7a). One plane of antisymmetry (the $x_2 - x_3$ plane) contains boundary fault A. The other plane of antisymmetry (the $x_1 - x_3$ plane) is perpendicular to the slip patch on A and extends through the patch center. No change in σ_{11} occurs along these planes of antisymmetry. Consequently,
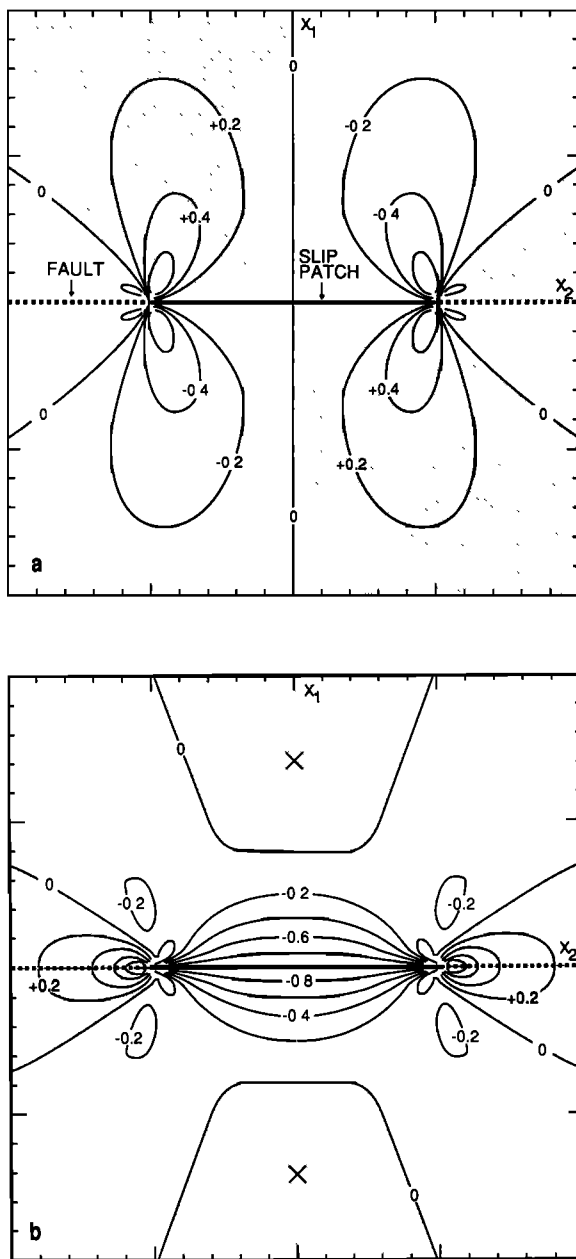
Fig. 7. (a) Change in σ_{11} and (b) change in σ_{12} about a left-lateral slip patch of unit half-length with a uniform unit stress drop. Shaded areas in Figure 7a, mark regions where σ_{11} becomes more compressive. Shaded areas in Figure 7b mark regions where σ_{12} increases. Cross at $x_1 \approx 1.4$ indicates location of maximum increase in σ_{12} along the x_1 axis. The remote shear stress σ_{12}^∞ is held constant during slip.

unslipped portion of fault A is increased strongly near the tips of the slip patch. Along the $x_1 - x_3$ plane, σ_{12} decreases near the slip patch, but increases above the ambient level farther than ~0.8 slip patch half-lengths from the slip patch. This phenomenon has been invoked as a mechanism for triggering off-fault aftershocks [Das and Scholz, 1981; Kostrov and Das, 1982]. The maximum increase of approximately (0.1) $(\sigma_{12}^\infty - \sigma_{12}^r)$ occurs about 1.4 slip patch half-lengths from the boundary fault [Pollard and Segall, 1987, Figure 8.10]. In part of this region of increased shear stress the resistance to slip is either unchanged or diminished. Thus, if a slip patch were on the verge of nucleating on fault B before slip nucleated on fault A, then slip on A would trigger the nucleation of slip on B.

So far, we have idealized the small distance over which a slip patch nucleates as a point. We note now that if a slip patch on A nucleates with a length greater than 2.5 times the distance between the boundary faults, then σ_{12} at an adjacent point on B will be decreased and a slip patch would be less likely to nucleate there. The proposed mechanism will be most effective in triggering slip if slip patches nucleate with a length less than 1.4 times the distance between the boundary faults. Thus the nucleation length of a slip patch relative to the spacing between faults determines to a large extent how one fault is likely to respond to slip on the other.

We have explicitly modeled the interaction between slip patches (Figure 8) using a boundary element method [e.g., Crouch and Starfield, 1983]. The fundamental solutions used in our model are given by Pollard and Holzhausen [1979]. In this method each slip patch is divided into intervals, and the prescribed boundary stress conditions on those intervals are solved for by successive iteration [Segall and Pollard, 1980]. The elastic boundary value solution of Pollard and Holzhausen [1979] was modified to require that the patch walls remain in contact.

Suppose the slip patches have grown such that their tips are approximately adjacent, in the manner shown in Figure 8. The slip patch on A lies in the third and fourth quadrants of Figure 8, and the slip patch on B lies in the first and second quadrants. Because of the symmetric distribution of the shear stress and the symmetric geometry of the slip patches, G_{II} will be the same at all four slip patch tips. However, the resistance to the propagation of slip G_{II}^{slip} will not be the same because of the antisymmetric distribution of σ_{11} (Figure 8a). The compression across fault A increases in the fourth quadrant but decreases in the third quadrant as a result of slip on B. Similarly, the compression across fault B increases in the second quadrant but decreases in the first quadrant as a result of slip on A. Thus a "stress barrier" arises (Figure 6c) which would increase G_{II}^{slip} and impede slip on fault B in the second quadrant and fault A in the fourth quadrant. In contrast, the tendency for slip to propagate is enhanced on A in the first quadrant and on B in the third quadrant. Thus, for left-lateral slip, the slip patches would tend to grow preferer-tially into a left-stepping configuration (Figure 6d). A

the resistance to slip would be unchanged along fault A and at the point on fault B nearest the slip patch on A. Near the x_1 axis in Figure 6a, the resistance to slip on fault B would be decreased in the first quadrant and increased in the second quadrant.

Slip also perturbs the shear stress parallel to the boundary faults (σ_{12}). The change in σ_{12} has a symmetric distribution, the $x_2 - x_3$ and $x_1 - x_3$ planes being the planes of symmetry (Figure 7b). The shear stress along the
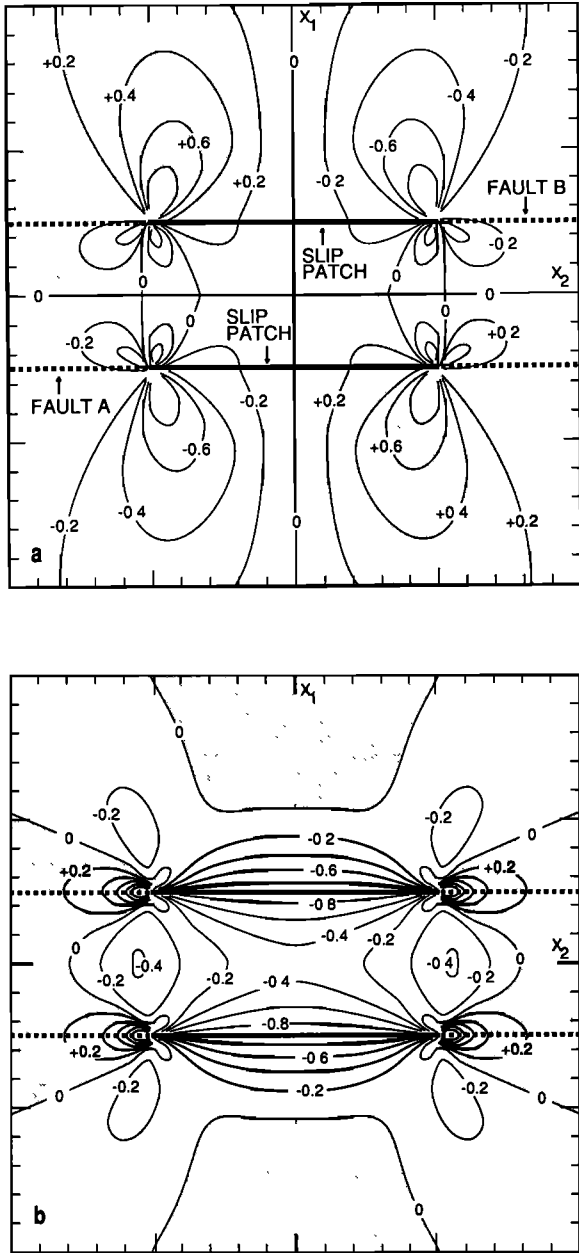
Fig. 8. (a) Change in σ_{11} and (b) change in σ_{12} about two slip patches with uniform unit stress drops. Shaded areas in Figure 8a mark regions where σ_{11} becomes more compressive. Shaded areas in Figure 8b mark regions where σ_{12} increases. The remote shear stress σ_{12}^∞ is held constant during slip.

right-stepping configuration would arise for right-lateral slip.

For the left-stepping configuration of Figure 6d, we will refer to the patch tips in the second and fourth quadrants as the inner tips, and the tips in the first and third quadrants as the outer tips. Because of the increased resistance to the propagation of slip encountered by the inner tips, tensile stress concentrations similar to those at the ends of small faults could be produced. As discussed above, these stress concentrations could lead to the generation of splay cracks. In this case, the splay cracks

would be preferentially directed into the fault zone, consistent with our observations.

Inwardly-directed splay cracks produced in this manner would tend not to cross the other boundary fault for three reasons. First, the ambient compressive stress acts to limit the distance a splay crack can propagate, so a splay crack would not necessarily be able to reach the other boundary fault (Figure 9a). Second, the compressive stress σ_{22} acting parallel to the boundary faults will be increased outside the fault zone by slip on the boundary fault toward which the splay crack grows (Figure 9a). Third, if a splay crack does intersect the other boundary fault, then the splay crack walls will tend to slide away from each other along the fault (Figure 9b). The leading edge of the splay crack would be blunted, drastically reducing the ability of the crack to propagate [Weertman, 1980; Keer and Chen, 1981]. The difficulty in propagating a splay crack across an adjacent boundary fault is consistent with the observed lack of splay cracks that cross boundary faults.

If the shear stress σ_{12}^r dropped to zero (Figure 5), then most of a slip patch would lie along a principal stress plane. Between slightly overlapping inner slip patch tips, trajectories of maximum compressive stress would approach the slip patches at right angles. Under these conditions, we would expect that a splay crack propagating from one slip patch would intersect the other patch at right angles. However, the most prominent fractures within the central portions of fault zone segments appear to intersect boundary faults at angles between 20° and 60° [Martel et al., 1988]. We therefore infer that the shear stress did not drop to zero during a typical slip event.

In contrast to the inner tips of the slip patches, propagation of the outer tips (Figure 6d) is enhanced by mechanical interaction. We suggest that the outer tips would tend to propagate as on the small faults. Propagation of the outer tips is likely to be impeded at the end of a fault zone segment, and we expect that stress concentrations could be produced there like those at the ends of small faults. The
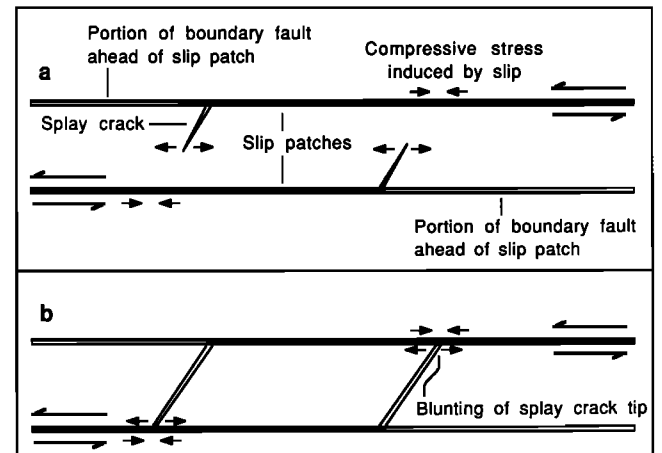

Fig. 9. Growth of a cross fracture as it (a) approaches and (b) intersects the opposite boundary fault. In Figure 9b the cross fracture walls pull apart, blunting the cross fracture tip.

resulting splay cracks would be directed out of the fault zone at segment ends. This is consistent with our observations as illustrated in Figure 2.

Two additional aspects of the faulting process remain to be included in the model of faulting described here. First, although we have identified a possible mechanism for triggering the nucleation of the second slip patch on a pair of boundary faults, we do not know specifically what mechanism is likely to have caused the first slip patch to nucleate. Second, the many slip events we postulate to produce the many fractures along a fault zone would require the fault to heal between events. The manner in which this occurs is not clear. Laboratory testing of large-scale samples that contain at least two parallel fractures filled with real fault material could shed some light on both these topics.

STRESS DROP AND SHEAR STRAIN RATE

Intriguingly, all boundary faults examined thus far are characterized by cataclastic textures, whereas all the small faults examined are characterized by mylonitic fabrics. This indicates that a common mechanism may cause extensive fracturing to develop between certain faults and cataclastic textures to develop in them. *Martel et al.* [1988] suggested that the transition from mylonitic fabrics to cataclastic textures in the boundary faults resulted from an increase in the shear strain rate across the boundary faults as adjacent small faults became inactive. We consider now whether an increase in displacement rate would promote fracturing between adjacent faults.

The relationship between the relative shear displacement across a slip patch (Δu_{II}) and the stress drop ($\sigma_{12}^\infty - \sigma_{12}^r$) is

$$\Delta u_{II} = 2(\sigma_{12}^\infty - \sigma_{12}^r)(1 - v)(c^2 - x_2^2)^{1/2}/\mu \qquad (4)$$

where v is Poisson's ratio, c is the slip patch half-length, x_2 is the distance from the slip patch center, and μ is the shear modulus [*Pollard and Segall*, 1987]. The expression can be solved for the displacement D at the slip patch center, where relative displacement is greatest

$$D = 2(\sigma_{12}^\infty - \sigma_{12}^r)(1 - v)c/\mu \qquad (5)$$

Differentiating equation (5) with respect to time t, and holding the stress drop during a given slip event constant yields

$$dD/dt = 2(\sigma_{12}^\infty - \sigma_{12}^r)(1-v)/\mu)(dc/dt) \qquad (6)$$

The term dc/dt is the rate at which the tips of a slip patch would propagate. Thus a larger stress drop is consistent with a greater displacement rate during a slip event. We note, however, that an increased displacement rate does not require an increased stress drop; a slip patch could instead lengthen at a greater rate. Still, if the stress drop during slip events were significantly greater for boundary faults than for small faults, then that could explain why slip on a boundary fault would have triggered slip on an adjacent fault (the other boundary fault) whereas slip on a

small fault would not. Because we rely on interactive slip between adjacent boundary faults to account for the extensive fracturing in simple fault zones, we suggest that differences in displacement rates during slip events on small faults and boundary faults could account indirectly for the differences in fracturing between small faults and boundary faults.

An alternative explanation for the lack of fracturing between closely spaced small faults is that the slip patches that nucleated along small faults were too long (greater than 2.5 times the distance to the adjacent fault) to trigger slip on an adjacent fault. This would imply that slip patches that nucleated along boundary faults were shorter than those along small faults. Experimental work on large samples, such as those used by *Okubo and Dieterich* [1984], that are modified to include two closely spaced faults could help decide which explanation is correct.

Simple fault zones generally are no more than a few meters wide, suggesting that the mechanical interaction between boundary faults usually was effective over distances no more than a few meters. This implies that many of the changes in stress associated with the growth of slip patches were small, and indeed the changes in σ_{11} and σ_{12} on one slip patch induced by a stress drop on another would be small relative to that stress drop (Figure 8). Thus, we rely on small changes in σ_{12} to have triggered slip and small changes in σ_{11} to explain why G_{II}^{slip} is less than G^{splay} in some cases but greater in others. We suggest that either G_{II}^{slip} was very sensitive to small changes in σ_{11} at the ambient pressure, which *Martel et al.* [1988] estimated as 100 MPa, or else that G_{II}^{slip} was only very slightly less than G^{splay} under ambient conditions.

ESTIMATES FOR STRESS DROP AND SHEAR FRACTURE ENERGY RELEASE RATE

The presence of many splay cracks along the simple fault zones suggests that many slip events occurred along the boundary faults. Assuming that each splay crack from a boundary fault represents one slip event, it is possible to estimate the average stress drop during a slip event along a boundary fault. Equation (5) gives the maximum displacement on an isolated slip patch. For two interacting and overlapping slip patches, equation (5) would approximate the maximum displacement on one of the slip patches within a factor of two. Equation (5) can be recast to solve for the stress drop

$$(\sigma_{12}^\infty - \sigma_{12}^r) = \mu D/2(1 - v)c \qquad (7)$$

Field measurements allow us to estimate D and c and arrive at an estimate for the stress drop. The maximum displacement across a slip patch can be estimated assuming that a large fraction of the maximum displacement during a slip event is accommodated by the opening of splay cracks. Splay cracks within simple fault zones typically are 0.2-0.5 mm wide, so we estimate the maximum relative displacement during a slip event to be about 1 mm. According to our model, roughly half of all slip patches should grow to lengths greater than segment half-lengths.
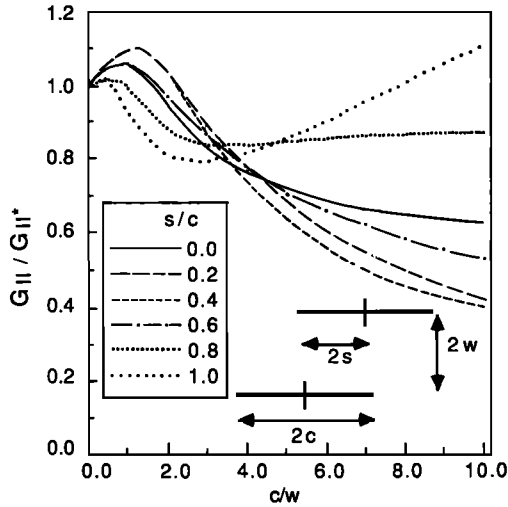
Fig. 10. Normalized values of G_{II} at the overlapped inner tips of two interacting slip patches (heavy lines). The slip patch length is 2c, the spacing between slip patch centers is 2s, and the spacing between boundary faults is 2w. The values of G_{II} are normalized by G_{II}^*, the value of G_{II} for a single slip patch of length 2c.

Therefore, a representative slip patch half-length would be one fourth the length of a simple fault zone segment, that is, 10 m. Using a shear modulus of 2×10^4 MPa, a Poisson's ratio of 0.25, 10 m for c and 1 mm for D, equation (7) yields an average stress drop of 1 MPa. This at the low end of the 1-10 MPa stress drop range associated with earthquakes [*Hanks*, 1977].

For the slip patch geometries of interest, our modified version of the solution of *Pollard and Holzhausen* [1979] indicates that the actual values of G_{II} at the inner slip patch tips (Figure 10) would be between 1.2 and 0.25 times the value given by equation (2). Substituting expression (7) for the stress drop into equation (2), the value of G_{II} is then given by

$$\frac{(0.25)\pi\mu D^2}{4c(1-v)} < G_{II} < \frac{(1.2)\pi\mu D^2}{4c(1-v)} \qquad (8)$$

Using the same values for μ, D, and v as above, and assuming that internally directed splay cracks formed where slip patches had half-lengths between 1 and 10 m, we arrive at an estimate of G_{II} prior to splay crack formation between 5×10^2 and 2×10^4 J/m². We note that this estimate comes from a perfectly elastic model in which the mechanical energy released is used solely to drive the slip patch. Along the actual faults, some energy would be expended in frictional sliding of splay cracks and through other nonelastic mechanisms. Thus the energy release rate associated solely with propagation of slip patches on the real faults would be no greater than the values given above.

Values of 5×10^2 - 2×10^4 J/m² for G_{II}^{slip} along boundary faults are roughly comparable to those obtained for the formation of shear fractures in intact laboratory samples of Westerly granite. *Wong* [1982] calculated G_{II} values between 10^3 and 10^5 J/m². His experiments were

conducted at temperatures between 150°C and 668°C and confining pressures of 80 and 350 MPa. These conditions probably bracket the temperatures and pressures under which slip occurred on the Mount Abbot faults. *Cox and Scholz* [1988] obtained a value of 5×10^2 J/m² from torque tests on cylinders of Westerly granite with no applied axial load. They recommend that this value be considered a lower bound on G_{II} and indicate that their results most properly apply to the initiation of shear fractures rather than the development of an equilibrium shear rupture. The apparent similarity between the experimental values and ours is somewhat surprising given that their values correspond to G_{II}^{shear} and not G_{II}^{slip}. One also might expect the shear fracture energy of intact granite to be quite different from a sheared assemblage of epidote, chlorite, and quartz.

Our estimate of G_{II}^{slip} is somewhat greater than the results indicated by the work of *Okubo and Dieterich* [1984]. Their work was conducted on simulated 2-m-long faults under normal stresses of 0.6 and 4 MPa. Extrapolating their findings to fault normal stresses of ~100 MPa yields G_{II} values between 25 and 100 J/m², at least an order of magnitude lower than ours. If the difference between their estimate of G_{II} and ours is due to the greater roughness of the Mount Abbot boundary faults, then one might expect the shear fracture energy for even larger faults to be markedly greater than 5×10^2 - 2×10^4 J/m².

Estimates of G_{II} for slip along major fault zones typically range from 10^6 to 10^8 J/m² [*Li*, 1987], more than two orders of magnitude higher than ours. A notable exception is the estimate of G_{II}^{slip} = 2.6×10^2 J/m² based on a creep event along a 6-km-long section of the San Andreas fault [*Rice and Simons*, 1976]. We suggest that the greater values of G_{II}^{slip} for fault zones larger than those we studied may reflect the greater structural complexity of large fault zones. Our observations indicate that propagating a shear fracture in-plane through massive granitic rock is extremely difficult. Even small bends and steps along simple fault zones apparently could cause slip patches to terminate. Given the much greater size of steps and bends which slip patches must propagate past along major fault zones, it is not surprising that propagation of slip along major fault zones would require energy release rates greater than on the small fault zones we have studied.

Summary

Fracture mechanics models for the nucleation, propagation, and termination of crack-like shear displacement discontinuities (slip patches) along pre-existing faults can account for the fracture structure observed along faults and fault zones in the Mount Abbot quadrangle of California. Along small left-lateral strike-slip faults, splay cracks are common only near fault ends. We infer that these cracks formed in response to slip patches that propagated to near the fault ends. Simple left-lateral fault zones consist of segments linked end-to-end. Many splay cracks project into a fault zone from its boundary faults, but except near segment ends, few project to the outside. If a

slip patch nucleated on one boundary fault over a distance less than the spacing between bounding faults, then the shear stress would rise at an opposite point on the second bounding fault and could trigger nucleation of a second slip patch there. The subsequent interaction of two such slip patches would favor propagation in a left-stepping echelon configuration. We suggest that critical tensile stress concentrations may have developed at the over-lapped (inner) tips of the slip patches where the resistance to slip propagation would be increased by interaction of the patches, resulting in cracks directed into the fault zone. The outer slip patch tips would have tended to pro-pagate to the end of a fault zone segment and there gen-erate cracks directed out of the fault zone. Using splay crack widths to approximate the slip per event and fault zone segment lengths to limit slip patch lengths, we esti-mate the average stress drops for slip events along the fault zones as ~1 MPa. We estimate the shear fracture energy release rate as $5 \times 10^2 - 2 \times 10^4$ J/m^2. This estimate is similar to those obtained from shear fracture of labora-tory samples, but orders of magnitude less than those for large fault zones. These results suggest that the shear frac-ture energy release rate increases as the structural com-plexity of fault zones increases.

REFERENCES

Andrews, D. J., Rupture propagation with finite stress in anti-plane strain, *J. Geophys. Res., 81,* 3575-3582, 1976.

Atkinson, B. K., Subcritical crack growth in geological materi-als, *J. Geophys. Res., 89,* 4077-4114, 1984.

Atkinson, B. K., and P. G. Meredith, Experimental fracture mechanics data for rocks and minerals, in *Fracture Mechanics of Rock,* edited by B. K. Atkinson, pp. 477-525, Academic, San Diego, Calif. 1987.

Brace, W. F., and E. G. Bombolakis, A note on brittle crack growth in compression, *J. Geophys. Res., 68,* 3709-3713, 1963.

Brace, W. F., and J. B. Walsh, Some direct measurements of the surface energy of quartz and orthoclase, *Am. Mineral., 47,* 1111-1122, 1962.

Cotterell, B., and J. R. Rice, Slightly curved or kinked cracks, *Int. J. Fract., 16,* 155-169, 1980.

Cox, S. J. D., and C. H. Scholz, Rupture initiation in shear frac-ture of rocks: An experimental study, *J. Geophys. Res., 93,* 3307-3320, 1988.

Crouch, S. L., and A. M. Starfield, *Boundary Element Methods in Solid Mechanics,* 322 pp., Allen and Unwin, London, 1983.

Das, S., and C. H. Scholz, Off-fault aftershocks caused by shear stress increase?, *Bull. Seismol. Soc. Am., 71,* 1669-1675, 1981.

Degraff, J. M., and A. Aydin, Dependence of columnar joint spacing and growth increment on cooling rate in lava flows (abstract), *Eos Trans. AGU, 67,* 1211, 1986.

Delaney, P. T., and D. D. Pollard, Deformation of host rocks and flow of magma during growth of minette dikes and breccia-bearing intrusions near Ship Rock, New Mexico, *U.S. Geol. Surv. Prof. Pap., 1202,* 61 pp., 1981.

Erdogan, F., and G. C. Sih, On the crack extension in plates under plane loading and transverse shear, *J. Basic Eng., 85,* 519-527, 1963.

Freund, L. B., The mechanics of dynamic shear crack propaga-tion, *J. Geophys. Res., 84,* 2199-2209, 1979.

Friedman, M., J. Handin, and G. Alani, Fracture-surface energy of rocks, *Int. J. Rock Mech. Min. Sci. Geomech. Abstr., 9,* 757-766, 1972.

Hanks, T. C., Earthquake stress drops, ambient tectonic stresses and stresses that drive plate motions, *Pure Appl. Geophys., 115,* 441-458, 1977.

Harris, R., and P. Segall, Detection of a locked zone at depth on the Parkfield, California segment of the San Andreas fault, *J. Geophys. Res., 92,* 7945-7962, 1987.

Ida, Y., Cohesive force across the tip of a longitudinal-shear crack and Griffith's specific surface energy, *J. Geophys. Res., 77,* 3796-3805, 1972.

Ida, Y., Stress concentration and unsteady propagation of longi-tudinal shear cracks, *J. Geophys. Res., 78,* 3418-3429, 1973.

Ingraffea, A. R., Mixed-mode fracture initiation in Indiana lime-stone and Westerly granite, Proc. U. S. Symp. Rock Mech., 22nd, 186-191, 1981.

Keer, L. M., and S. H. Chen, The interaction of a pressurized crack with a joint, *J. Geophys. Res., 86,* 1032-1038, 1981.

Kostrov, B. V., and S. Das, Idealized models of fault behavior prior to dynamic rupture, *Bull. Seismol. Soc. Am., 72,* 679-703, 1982.

Kulander, B. R., C. C. Barton, and S. L. Dean, *The Application of Fractography to Core and Outcrop Fracture Investigations,* 174 pp., Morgantown Energy Technology Center, Morgan-town, W. Va., 1979.

Lawn, B. R., and T. R. Wilshaw, *Fracture of Brittle Solids,* 204 pp., Cambridge University Press, New York, 1975.

Li, V. C., Mechanics of shear rupture applied to earthquake zones, in *Fracture Mechanics of Rock,* edited by B. K. Atkin-son, pp. 351-428, Academic, San Diego, Calif., 1987.

Martel, S. J., D. D. Pollard, and P. Segall, Development of simple strike-slip fault zones in granitic rock, Mount Abbot quadran-gle, Sierra Nevada, California, *Geol. Soc. Am. Bull., 100,* 1451-1465, 1988.

Meredith, P. G., and B. K. Atkinson, Fracture toughness and sub-critical crack growth during high-temperature tensile defor-mation of Westerly granite and Black gabbro, *Phys. Earth Planet. Inter., 39,* 33-51, 1985.

Nemat-Nasser, S., and H. Horii, Compression-induced nonplanar crack extension with application to splitting, exfoliation, and rockburst, *J. Geophys. Res., 87,* 6805-6821, 1982.

Okubo, P. G., and J. H. Dieterich, Fracture energy of stick-slip events in a large scale biaxial experiment, *Geophys. Res. Lett., 8,* 887-890, 1981.

Okubo, P. G., and J. H. Dieterich, Effects of fault properties on frictional instabilities produced on simulated faults, *J. Geo-phys. Res., 89,* 5817-5827, 1984.

Palmer, A. C., and J. R. Rice, The growth of slip surfaces in the progressive failure of over-consolidated clay, *Philos. Trans. R. Soc. London, 332,* 527-548, 1973.

Peck, L., R. C. Nolen-Hoeksema, C. C. Barton, and R. B. Gor-don, Measurement of the resistance of imperfectly elastic rock to the propagation of tensile cracks, *J. Geophys. Res., 90,* 7827-7836, 1985a.

Peck, L., C. C. Barton, and R. B. Gordon, Microstructure and the resistance of rock to tensile fracture, *J. Geophys. Res., 90,* 11, 533-11,546, 1985b.

Pollard, D. D., and G. Holzhausen, On the mechanical interac-tion between a fluid-filled fracture and the Earth's surface, *Tectonophysics, 53,* 27-57, 1979.

Pollard, D. D., and P. Segall, Theoretical displacements and stresses near fractures in rocks: With applications to faults, joints, veins, dikes, and solution surfaces, in *Fracture Mechanics of Rock,* edited by B. K. Atkinson, pp. 277-349, Academic, San Diego, Calif., 1987.

Pollard, D. D., P. T. Delaney, W. A. Duffield, E. T. Endo, and A. T. Okamura, Surface deformation in volcanic rift zones, *Tectonophysics, 94,* 541-584, 1983.

Rice, J. R., and D. A. Simons, The stabilization of spreading shear faults by coupled deformation-diffusion effects in fluid-infiltrated porous materials, *J. Geophys. Res., 81,* 5322-5334, 1976.

Rodgers, D. A., Analysis of pull-apart basin development produced by en echelon strike-slip faults, in *Sedimentation in Oblique-Slip Mobile Zones, Spec. Publ. 4,* edited by P. F. Ballance and H. G. Reading, pp. 27-41, International Association of Sedimentologists, Oxford, England, 1980.

Rubin, A. M., and D. D. Pollard, Origins of blade-like dikes in volcanic rift zones, Volcanism in Hawaii, vol. 2, edited by R. W. Decker, T. L. Wright, and P. H. Stauffer, *U. S. Geol. Surv. Prof. Pap., 1350,* 1449-1470, 1987.

Rudnicki, J. W., Fracture mechanics applied to the Earth's crust, *Annu. Rev. Earth Planet. Sci., 8,* 489-525, 1980.

Ryan, M. P., and C. G. Sammis, Cyclic fracture mechanisms in cooling basalt, *Geol. Soc. Am. Bull., 89,* 1295-1308, 1978.

Segall, P., Formation and growth of extensional fracture sets, *Geol. Soc. Am. Bull., 95,* 454-462, 1984.

Segall, P., and D. D. Pollard, Mechanics of discontinuous faults, *J. Geophys. Res., 85,* 4337-4350, 1980.

Segall, P., and D. D. Pollard, Joint formation in granitic rock of the Sierra Nevada, *Geol. Soc. Am. Bull., 94,* 563-575, 1983*a.*

Segall, P., and D. D. Pollard, Nucleation and growth of strike-slip faults in granite, *J. Geophys. Res., 88,* 555-568, 1983*b.*

Segall, P., and C. Simpson, Nucleation of ductile shear zones on dilatant fractures, *Geology, 14,* 55-59, 1986.

Sibson, R. H., Stopping of earthquake ruptures at dilational fault jogs, *Nature, 316,* 248-251, 1985.

Stein, R. S., and M. Lisowski, The Homestead Valley earthquake sequence, California: Control of aftershocks and postseismic deformation, *J. Geophys. Res., 88,* 6477-6490, 1983.

Thatcher, W., Systematic inversion of geodetic data in central California, *J. Geophys. Res., 84,* 2283-2295, 1979.

Weertman, J., The stopping of a rising, liquid-filled crack in the Earth's crust by a freely slipping horizontal joint, *J. Geophys. Res., 85,* 967-976, 1980.

Wong, T.-F., Micromechanics of faulting in Westerly granite, *Int. J. Rock Mech. Min. Sci. Geomech. Abstr., 19,* 49-64, 1982.

Wong, T.-F., On the normal stress dependence of the shear fracture energy, in *Earthquake Source Mechanics, Maurice Ewing Ser.,* vol. 6, edited by S. Das, J. Boatwright, and C. H. Scholz, pp. 1-11, AGU, Washington, D.C., 1986.

S. J. Martel, Earth Sciences Division, Lawrence Berkeley Laboratory, One Cyclotron Road, Berkeley, CA 94720.

D. D. Pollard, Departments of Applied Earth Sciences and Geology, Stanford University, Stanford, California 94305